ROYAL SOCIETY
OF CHEMISTRY

PAPER

Check for updates

Circularly polarized organic room temperature phosphorescence activated by liquid crystalline polymer networks†

Ao Huang,[a] Jiang Huang,[a] Hui-Ying Luo,[a] Zhi-Wang Luo,[a] Pu Wang,*[a] Ping Wang,*[a] Yan Guan[b] and He-Lou Xie (ID) *[a]

Circularly polarized luminescent (CPL) materials have attracted much attention due to their potential applications in 3D imaging, anti-counterfeiting, *etc.* However, it is still a great challenge to achieve circularly polarized room temperature phosphorescence (CPRTP). In this work, a series of chiral compounds (denoted as (R/S)-B-*n*-CzO, *n* = 4, 8 and 12) are successfully designed and synthesized combining binaphthol and carbazole–dibenzofuran for the fabrication of CPRTP materials. The resultant compounds show excellent luminescence behaviour in both solution and the solid state with absolute fluorescence quantum yields of up to 52.97%. Due to the existence of a chiral group, these compounds show circular dichroism (CD) in solution, but no CPL behaviour is observed. Furthermore, this kind of compound is doped into a commercial liquid crystalline monomer (2-methyl-1,4-phenylene bis (4-(((4-(acryloyloxy) butoxy) carbonyl) oxy) benzoate, LC-242)) to fabricate CPRTP materials through liquid crystal (LC) self-assembly and a confined phosphorescent moiety by UV light cross-linking the monomer. As a result, the obtained liquid crystalline polymer network shows CPRTP behaviour with the largest luminescence dissymmetry (g_{lum}) value of +0.098. This provides a meaningful design idea for the preparation of CPRTP materials.

Introduction

Circularly polarized luminescent (CPL) materials with outstanding optical sensitivity and spatial resolution have promising applications in asymmetric catalysis,[1,2] data storage,[3,4] 3D displays,[5,6] and optical encryption.[7–9] The performance of CPL materials is evaluated using dissymmetry (g_{lum}) values and photoluminescence quantum efficiency (PLQY).[4,10–13] In recent years, different systems of CPL materials have been developed,

such as organic crystals,[14,15] self-assembled systems,[16] metal complexes,[17] and polymers.[18] Organic small molecules with specific structures can spontaneously organize or aggregate into stable and regular structures under non-covalent interactions, which greatly amplifies chirality and improves the g_{lum} value by controlling the spatial arrangement of structural units.[19] Thus, the supramolecular self-assemblies of organic molecules as excellent CPL materials show high g_{lum} values and luminescence efficiency.[20] The current research on CPL properties is mainly focused on fluorescent organic luminescent groups, but achieving long-lived organic room-temperature phosphorescent (RTP) materials with CPL remains a great challenge.

RTP materials with long-lived triplet-state excitons and large Stokes shifts have received much attention for their extensive applications.[21–23] Compared with the traditional inorganic metal RTP materials, organic RTP materials are of low cost, show environmental friendliness and can be easily synthesised.[24–32] Thus, organic RTP materials have gained great attention in recent decades.[33–38] Currently, efficient organic RTP materials can be obtained in two ways. Firstly, introducing carbonyl units and heavy atoms into the targeted molecules produces strong spin–orbit coupling (SOC), which leads to high intersystem crossing rates and more triplet-state excitons;[39] and secondly, suppressing the non-radiative transition of triplet-state excitons can be realized

[a] *Key Lab of Environment-friendly Chemistry and Application in Ministry of Education, and Key Laboratory of Advanced Functional Polymer Materials of Colleges, Universities of Hunan Province and College of Chemistry, Xiangtan University, Xiangtan Hunan, 411105, China. E-mail: 90wangpu@xtu.edu.cn, 395658023@qq.com, xhl20040731@163.com*

[b] *Beijing National Laboratory for Molecular Sciences, Key Laboratory of Polymer Chemistry and Physics of Ministry of Education, Center for Soft Matter Science and Engineering, College of Chemistry and Molecular Engineering, Peking University, Beijing, 100871, China*

† Electronic supplementary information (ESI) available: Materials, instruments and measurements; NMR, MALDI-TOF and 1D XRD spectra of (R/S)-B-*n*-CzO; DSC, POM and FT-IR results of M-(R/S)-B-*n*-CzO and P-(R/S)-B-*n*-CzO; UV-vis, PL, CD, CPL and fluorescence quantum yield results of (R/S)-B-*n*-CzO in different states; PL, CD, CPL and lifetime decay curve results of P-(R/S)-B-*n*-CzO; and PL, POM, CD and CPL results of (R/S)-B-*n*-CzO-5%@E7. See DOI: https://doi.org/10.1039/d2tc04829a
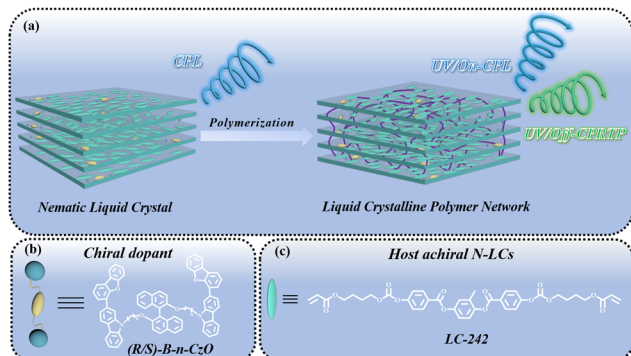
Fig. 1 (a) Schematic diagram of the preparation route for the liquid crystalline polymer network with CPRTP. Molecular structures of the chiral dopant ((R/S)-B-n-CzO) (b) and the host N-LC (LC-242) (c).

through crystallization, H-aggregation, polymer matrix, *etc.*[40–42] Although organic RTP materials with a long lifetime and high luminescence efficiency have achieved great progress, organic RTP materials with CPL properties are still rarely explored.[43–49]

In order to achieve CPRTP, the current strategy is to integrate the chiral center with the phosphorescent emitting group, which is assembled to amplify an ordered structure and realize a high g_{lum} value. Liquid crystal (LC) is a typical fluid with a long-range ordered structure, which is conducive to the preparation of efficient CPL materials.[50–52] It has been demonstrated that chiral nematic liquid crystals (N*-LCs) with high optical activity and a tunable pitch have been recently used to construct CPL materials with high g_{lum} values.[53,54] Herein, we intend to prepare excellent CPRTP materials using a liquid crystalline polymer network (Fig. 1a). Firstly, we designed and prepared a series of compounds (R/S)-B-n-CzO with a chiral center binaphthol and a non-chiral luminescent group of carbazole–dibenzofuran (Fig. 1b). Furthermore, the resultant compounds (R/S)-B-n-CzO were doped into a liquid crystalline monomer (2-methyl-1,4-phenylene bis (4-(((4-(acryloyloxy)butoxy)carbonyl)oxy) benzoate, LC-242)) (Fig. 1c). After complete mixing and annealing, the mixtures were further cross-linked under UV light. The resulting liquid crystalline polymer network showed green phosphorescence and high CPL properties with a fluorescence $|g_{lum}|$ value up to 0.097 and a phosphorescence $|g_{RTP}|$ of 0.098.

Experimental

Synthesis

The synthetic route of (R/S)-B-n-CzO is shown in Scheme 1. The synthesis process of different compounds was similar. Herein, we use the synthesis of (R)-2,2′-bis(4-(2-(dibenzo[b,d]furan-4-yl)-9H-carbazol-9-yl)butoxy)-1,1′-binaphthalene ((R)-B-4-CzO) as an example to describe this procedure. Below is a description of the synthesis information in detail. The relevant synthesis information is provided in the ESI† for additional compounds (Fig. S1 and S2).
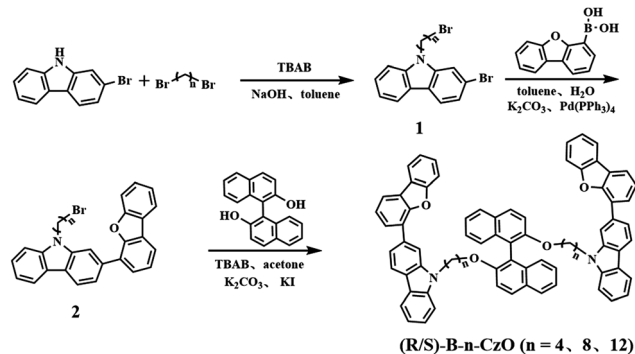
Scheme 1 Synthetic route of the compounds (R/S)-B-n-CzO.

Synthesis of 2-bromo-9-(4-bromobutyl)-9H-carbazole (1)

A 250 mL round bottom flask was filled with 2-bromocarbazole (0.2 g, 0.8 mmol), 1,4-dibromobutane (0.96 ml, 8 mmol), tetrabutylammonium bromide (TBAB) (0.05 g, 0.16 mmol), 50% NaOH aqueous solution (5 g NaOH, 5 mL H$_2$O) and 30 mL of toluene. The reaction mixture was further stirred at 45 °C for 10 hours. After the reaction completed, it was cooled to room temperature. Then the obtained products were dissolved in dichloromethane, followed by several washings with water. Following drying over sodium sulfate, the extracted organic phase was solvent-free under reduced pressure. Dichloromethane/petroleum ether (1 : 4, v/v) was used as the eluent in column chromatography to further purify the crude product, which produced compound **1** as a white solid with an 84% yield. ^{1}H NMR (CDCl$_3$, ppm) δ (ppm): 8.06 (d, 1H), 7.94 (d, 1H), 7.54 (d, 1H), 7.49 (t, 1H), 7.40 (d, 1H), 7.34 (dd, 1H), 7.25 (t, 1H), 4.31 (t, 2H), 3.40 (t, 2H), 2.06 (m, 2H), 1.92 (m, 2H).

Synthesis of 9-(4-bromobutyl)-2-(dibenzo[b,d]furan-4-yl)-9H-carbazole (2)

The synthesis process is detailed in our previous work.[55]

Synthesis of (R)-2,2′-bis(4-(2-(dibenzo[b,d]furan-4-yl)-9H-carbazol-9-yl)butoxy)-1,1′-binaphthalene ((R)-B-4-CzO)

A mixture of compound **2** (1.03 g, 2.2 mmol), (R)-1,1′-Bi-2-naphthol (0.29 g, 1.0 mmol), potassium carbonate (0.83 g, 6 mmol), potassium iodide (0.0083 g, 0.05 mmol), TBAB (0.02 g, 0.05 mmol) and 30 mL of acetone was added to a 100 mL round-bottomed flask. Further stirring and a 24 hour reflux process at 65 °C were performed on the reaction mixture. After the completion of the reaction, the mixture was filtered off and the solvent was removed by evaporation. Dichloromethane/petroleum ether (1 : 1, v/v) was used as the eluent in column chromatography to further purify the crude product, which produced (R)-B-4-CzO as a white solid with an 88% yield. ^{1}H NMR (CDCl$_3$) δ (ppm): 8.22 (d, 1H, Ar-H), 8.13 (d, 1H, Ar-H), 7.96 (dd, 1H, Ar-H), 7.91 (dd, 1H, Ar-H), 7.77 (dd, 1H, Ar-H), 7.66 (dd, 1H, Ar-H), 7.59 (d, 1H, Ar-H), 7.49 (d, 1H, Ar-H), 7.36 (tt, 6H, Ar-H), 7.22 (t, 1H, Ar-H), 7.06–6.90 (m, 4H, Ar-H), 6.90 (d, 1H, Ar-H), 3.84–3.54 (m, 4H, O–CH$_2$–, N–CH$_2$–), 1.31–1.19 (m, 4H, –CH$_2$–CH$_2$–).

This journal is © The Royal Society of Chemistry 2023

J. Mater. Chem. C, 2023, **11**, 4104–4111 | **4105**

^{13}C NMR: 156.22 (binaphthyl CH$_2$=C–O), 154.45, 141.11 (dibenzofuran C–O), 140.77, 133.88, 123.31, 122.81, 120.69, 120.55, 120.49, 111.82, 109.26, 108.76 (carbazole CH$_2$=C–C), 134.14, 125.93 (carbazole C–N), 130.94, 128.96, 128.88, 127.71, 127.21, 127.02, 125.78, 122.53, 119.43 (binaphthyl CH$_2$=C–C), 129.21, 127.30, 125.45, 124.97, 124.36, 123.32, 122.73, 120.76, 118.95, 115.85 (dibenzofuran CH$_2$=C–C), 69.59 (O–C–C), 43.14 (N–C–C), 27.14, 25.51 (–CH$_2$–).

MS: MALDI-MS (m/z): [M]$^+$ Calcd for C$_{76}$H$_{56}$N$_2$O$_4$, 1060.42; Found, 1060.17.

The preparation of the liquid crystalline polymer network

The LC monomer LC-242, chiral dopant ((R)-B-4-CzO), and photoinitiator 2,2-dimethoxy-2-phenylacetophenone (DMPA) with a mass ratio of 98 : 1 : 1 was dissolved in dichloromethane and then sonicated for two minutes. In order to prepare a dry and uniform LC mixture, the solvent naturally evaporated at ambient temperature. The LC mixture was injected into a 2.5 μm laboratory-prepared LC cell under a capillary force at 90 °C and slowly cooled (1 °C min^{-1}) to 75 °C. Then, the LC mixture was photopolymerized using a UV lamp (8 mW·cm^{-2}, λ = 365 nm; LP-40A; LUYOR Corporation) at 75 °C to obtain a liquid crystalline polymer network.

Results and discussion

Luminescence behaviour of compounds in the solid state and solution

The photophysical properties of the compounds were investigated in both THF solution and the solid state. These compounds showed similar UV-vis absorption spectra in the THF solution and the solid state (Fig. S3, ESI†). The absorption bands at 230–290 nm were assigned to the π–π* transition of the binaphthyl moiety, while the absorption peak at 320 nm was ascribed to the carbazole–dibenzofuran unit.[56] Furthermore, the emission behaviour was investigated. Apparently, the maximum fluorescence emission peak of (R/S)-B-n-CzO in the THF solution was located at 410 nm (Fig. 2a and Fig. S13, ESI†), which was attributed to the carbazole–dibenzofuran unit. The emission peaks of (R/S)-B-n-CzO in the thin films were located at 416–420 nm, showing a slightly bathochromic-shift compared to those in solution, which is due to the π–π stacking interaction of the compounds in the solid state (Fig. 2b). Interestingly, the compounds (R/S)-B-n-CzO still emitted strong blue fluorescence in the solid state, without aggregation-caused quenching behaviour. Moreover, the fluorescence quantum yields (Φ_F) of the compounds in the THF solution were 47.58%, 48.27%, 47.41%, 46.62%, 47.42% and 46.98% for (R)-B-4-CzO, (S)-B-4-CzO, (R)-B-8-CzO, (S)-B-8-CzO, (R)-B-12-CzO and (S)-B-12-CzO, respectively (Fig. 2c). Furthermore, the Φ_F of the powders were 52.97%, 50.45%, 42.13%, 44.82%, 40.29% and 25.61% for (R)-B-4-CzO, (S)-B-4-CzO, (R)-B-8-CzO, (S)-B-8-CzO, (R)-B-12-CzO and (S)-B-12-CzO, respectively (Fig. 2d). Clearly, these compounds showed high luminescence efficiency in both solution and the solid state.
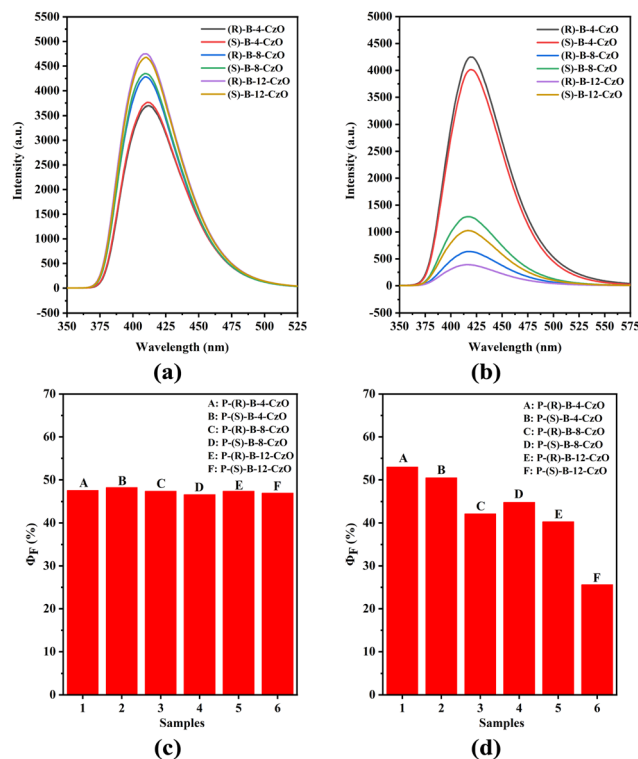

Fig. 2 Fluorescence emission spectra of (R/S)-B-n-CzO in solution (a) and films (b). Fluorescence quantum yields of (R/S)-B-n-CzO in solution (c) and the solid state (d).

In order to gain insight into the observed luminescence properties of the compounds, density functional theory (DFT) and time-dependent DFT (TD-DFT) were utilized to explore the geometrical structures of the ground S$_0$ and the singlet excited S$_1$ states. Since the chiral core has no any effect on the luminescence intensity, the R-type samples showed the same luminescent group as the S-type samples. So, we chose the R-type samples as the example to illustrate the phenomenon. In the S$_0$ state, all compounds adopted a twisted conformation. The frontier orbitals and oscillator strength (f) of the (R)-B-4-CzO, (R)-B-8-CzO and (R)-B-12-CzO molecules were calculated to elucidate the nature of the S$_1$ → S$_0$ emission. Fig. 3a illustrates the highest occupied molecular orbital (HOMO) and the lowest unoccupied molecular orbital (LUMO) of three molecules for the S$_0$ state at the S$_1$ optimized geometries. The oscillator strengths (f) of S$_1$ → S$_0$ transitions for (R)-B-4-CzO, (R)-B-8-CzO and (R)-B-12-CzO molecular were 0.27, 0.65 and 0.66, respectively. The root-mean-square displacement (RMSD) values between the optimized S$_0$ and S$_1$ states of (R)-B-4-CzO, (R)-B-8-CzO and (R)-B-12-CzO were 0.32 Å, 0.32 Å and 0.67 Å, respectively. Obviously, the large f and smaller RMSD values endowed the compound higher luminous intensity.[57] All these compounds had large f values, which lead to them exhibit a strong fluorescence emission in the solution state. The powder X-ray diffraction (XRD) showed that all compounds presented a diffuse diffracted halo (Fig. 3b and Fig. S12, ESI†), which indicated that these compounds could not present excellent
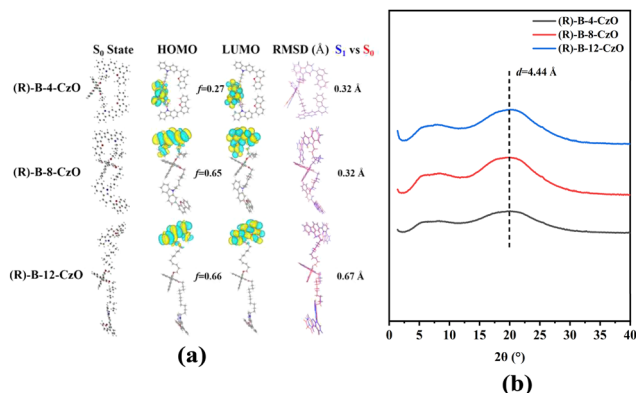
4106 | J. Mater. Chem. C, 2023, 11, 4104–4111

This journal is © The Royal Society of Chemistry 2023

Fig. 3 (a) The optimization structure in the ground state, frontier molecular orbitals (HOMO and LUMO) for the S_0 state at the S_1 optimized geometries, and RMSD (S1 *vs.* S0) of (R)-B-*n*-CzO. (b) Powder XRD pattern of solid powder (R)-B-*n*-CzO.

crystal density packing due to the large steric hindrance. The diffracted halo at $2\theta = 20.0°$ further demonstrated only weak π–π stacking in the solid state, which maintained the excellent emission in the solid state.[58,59] These results confirmed that the compounds (R/S)-B-*n*-CzO showed strong emission behaviours in the solution and the solid state.

In our previous works,[60] we used the luminescent group carbazole–dibenzofuran to fabricate high-efficiency phosphorescent polymers. Herein, the synthetic compounds contained not only the luminescent group carbazole–dibenzofuran but also the chirality group binaphthol. Thus, we further investigated their chiral and CPL behaviours. All the compounds exhibited similar Cotton effects at 290 nm in the short wavelength region in THF solution, which can be regarded as the characteristic absorption of chiral binaphthyl moieties (Fig. S4a, ESI†). The Cotton effect can be observed at about 320 nm, proving that the chirality was transferred intramolecularly from the chiral binaphthyl moiety to carbazole–dibenzofuran.[48] Moreover, all enantiomeric isomers exhibited mirror image CD signals. The CD spectra of solid films for all samples were similar to those in solution (Fig. S4b, ESI†). However, the CPL signal of the compounds was not detected in both solution and the film state (Fig. S4c and d, ESI†), which implied that even though the chirality was transferred to the luminous group in the excited state, and the existence of energy dissipation making it impossible for the CPL spectrometer to detect it.

The fabrication of the phosphorescent liquid crystalline polymer network

It is well known that binaphthyl derivatives have a strong helical twisting power and good miscibility with LC. At the same time, LC as a self-assembly fluid could form long-range ordered structures to amplify the CPL behaviour with high g_{lum} values. In this work, we chose the liquid crystalline monomer LC-242 as the matrix because it contained two vinyls to form the density cross-linking polymer network after polymerization, which encouraged the phosphorescent behaviour. Herein, 1wt% of the chiral dopants (R/S)-B-*n*-CzO were added to the
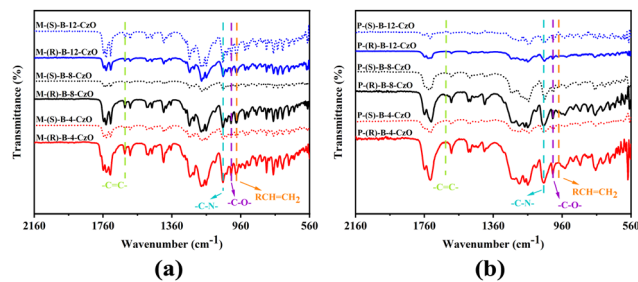

Fig. 4 FT-IR Spectra of (a) M-(R/S)-B-*n*-CzO and (b) P-(R/S)-B-*n*-CzO.

non-chiral liquid crystalline monomer LC-242 to prepare samples M-(R/S)-B-*n*-CzO. The samples of M-(R/S)-B-*n*-CzO were fully annealed to promote the LC ordered structure development. Then, the obtained LC mixture with the LC ordered structure was polymerized under UV light irradiation to prepare the liquid crystalline polymer network samples P-(R/S)-B-*n*-CzO. The obtained liquid crystalline polymer networks of P-(R/S)-B-*n*-CzO were first confirmed by Fourier transform infrared spectroscopy (FT-IR). Before polymerization, two peaks at 1650 cm^{-1} and 980 cm^{-1} for M-(R/S)-B-*n*-CzO were observed, which was attributed to the stretching vibrational peak of C=C and the bending vibrational peak of C=C–H (Fig. 4a). After polymerization, the above two peaks were disappeared and the other characteristic peaks remain unchanged, which indicated that the liquid crystal monomer LCL-242 had been completely polymerized (Fig. 4b). However, the bending vibrational peaks of C–N at 1057 cm^{-1} and C–O at 1010 cm^{-1} of the compound (R/S)-B-*n*-CzO did not change after polymerization, which proved that the compound existed stably and its structure did not change before and after polymerization.

Subsequently, the phase behaviour of the obtained polymer network was further investigated. Differential scanning calorimetry (DSC) results showed that the polymers P-(R/S)-B-*n*-CzO presented no phase transition peak during the whole heating process and the cooling process (Fig. 5a), which indicated that
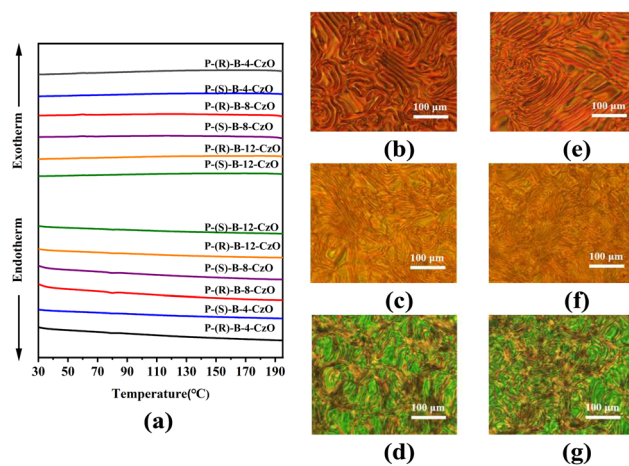

Fig. 5 (a) DSC traces of P-(R/S)-B-*n*-CzO. (b–g) POM images of the mixture containing (b) P-(R)-B-4-CzO, (c) P-(R)-B-8-CzO, (d) P-(R)-B-12-CzO, (e) P-(S)-B-4-CzO, (f) P-(S)-B-8-CzO and (g) P-(S)-B-12-CzO.

This journal is © The Royal Society of Chemistry 2023

J. Mater. Chem. C, 2023, **11**, 4104–4111 | **4107**

the density crosslinking structure had been stably formed. Polarized optical microscopy (POM) showed that all samples P-(R/S)-B-n-CzO presented a typical fingerprint texture, which indicated that the chiral molecules induced the LC monomer to form a helical structure. Moreover, these fingerprint textures would not disappear until the decomposition temperature, and always remained unchanged during the whole heating and cooling processes (Fig. 5b–g). These results demonstrated that the stable crosslinking liquid crystalline polymer network has been formed, which could provide the restricted environment for the luminescent compound (R/S)-B-n-CzO and promote the RTP generation.

The photophysical properties of the polymer network P-(R/S)-B-n-CzO were further studied. The maximum fluorescence emission peaks of samples P-(R/S)-B-n-CzO were almost unchanged at 405 nm compared with that of (R/S)-B-n-CzO (Fig. 6a). The green afterglow with a duration time of 6 ~ 11 s for the samples P-(R/S)-B-n-CzO could be observed by the naked eye, which indicated the generation of RTP (Fig. 6b). The phosphorescence spectra of P-(R/S)-B-n-CzO showed that the maximum phosphorescence emission peaks were located at 520 nm and 545 nm (Fig. 6c). This result demonstrated that the density cross-linked network formed by the polymerization of the liquid crystal monomer LC-242 had successfully stabilized triplet excitons and produced excellent room temperature phosphorescence. And all samples exhibited long-lived phosphorescence with lifetimes of 0.77 ~ 1.08 s (Fig. 6d). Obviously, the cross-linked polymer network structure could restrict the molecular motion of the compounds,

suppressed the non-radiative transition, and effectively shielded the quencher to promote the RTP emission.[61–63]

Circularly polarized organic room temperature phosphorescence

The distinct fingerprint texture demonstrated the chiral structure in these polymers. Mirror-image bands in the CD spectra showed that P-(R/S)-B-n-CzO was a pair of enantiomers, which implied the chirality of the samples in the ground state and agreed well with the absorption bands of the compounds in THF solution (Fig. 7a). These phenomena indicated that the P-(R/S)-B-n-CzO effectively displayed the chirality due to the intrinsic axial chirality of the binaphthol unit. Since the resulting chiral enantiomers P-(R/S)-B-n-CzO could exhibit the fluorescence emission in both solution and the solid state, we speculated all samples could show the CPL behaviour. So, the chiral features in the excited state were further investigated by CPL spectra. The CPL signal of P-(R/S)-B-n-CzO at approximately 410 nm corresponded to the maximum fluorescence emission wavelength of (R)-B-n-CzO (Fig. 7b, Fig. S5 and S14, ESI†), which proved that the samples showed fluorescence CPL. Notably, P-(R)-B-n-CzO showed the positive fluorescence CPL signal, while P-(S)-B-n-CzO exhibited a chiral inverse, *i.e.*, the negative fluorescence CPL signal. And their g_{lum} also in the order of magnitudes of 10^{-2} showed mirror symmetry, which corresponded to the CPL curve (Fig. 7c).

To explore the origin of the inversed CPL signals, we further carefully investigated the textures of the samples P-(R/S)-B-n-CzO. However, we could not find the whole screw senses of the liquid crystalline polymer network films, because the intensity crosslinking lead to the destruction of the large LC domain. Thus, we used room temperature LC E7 to dope with the compounds (R/S)-B-4-CzO to observe screw orientation. As described in
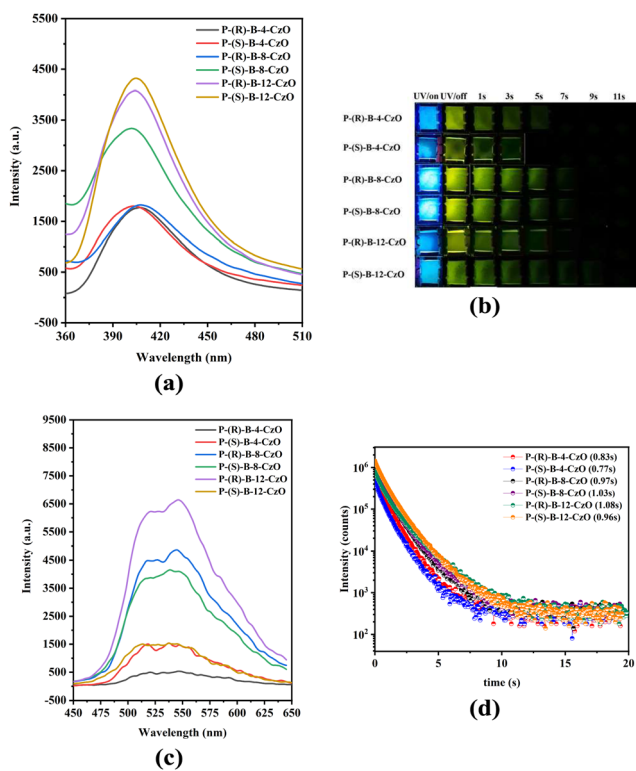

Fig. 6 (a) Fluorescence emission spectra. (b) Photographs of luminescence at different times after UV irradiation switch. (c) Phosphorescence emission spectra. (d) Lifetime decay curve of P-(R/S)-B-n-CzO.
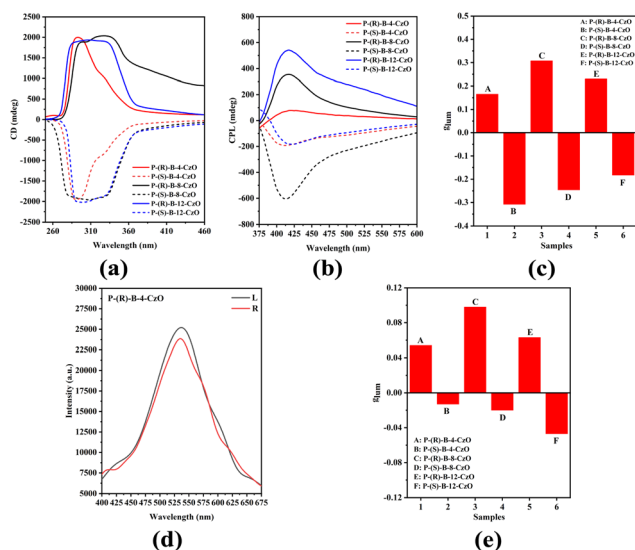

Fig. 7 (a) CD spectra of P-(R/S)-B-n-CzO. (b) CPL spectra and (c) g_{lum} values of P-(R/S)-B-n-CzO. (d) Phosphorescence emission spectra of P-(R)-B-4-CzO recorded with an L-CPF or R-CPF. (e) g_{RTP} values of P-(R/S)-B-n-CzO.

4108 | *J. Mater. Chem. C*, 2023, **11**, 4104–4111

This journal is © The Royal Society of Chemistry 2023

Fig. S7a and b (ESI†), 5wt% (R)-B-4-CzO and 5wt% (S)-B-4-CzO induced N*-LCs exhibit clockwise and counter clockwise screw orientations, respectively. The screw senses of N*-LCs coincided with the signals of CPL and CD spectra. It is evident that the stereospecific intermolecular interactions between the dinaphthyl group of the chiral dopants and the surrounding N-LC molecules control the screw sensing of N*-LC. Previous works have demonstrated that chiral binaphthyl enantiomer derivatives exhibited opposing helicity in both *cis* and *trans* conformations.[64] The dihedral angle (θ) of the binaphthyl ring affected the derivative helicity. The (R)-binaphthyl derivatives showed the (R)-cisoid conformation ($0° < \theta < 90°$) and (R)-transoid conformation ($90° < \theta < 180°$), which corresponded to (M)-helicity and (P)-helicity, respectively. Correspondingly, the (S)-binaphthyl derivatives showed the (S)-cisoid conformation ($0° < \theta < 90°$) and (S)-transoid conformation ($90° < \theta < 180°$), which corresponded to (P)-helicity and (M)-helicity, respectively. For the dopants, both the dihedral angles of (R)-B-n-CzO and (S)-B-n-CzO were smaller than 90°, exhibiting an M-helicity and a P-helicity in N-LCs, respectively. As a result, the chirality inversion phenomenon could be observed in these samples.

Since the CPRTP of most organic compounds was currently undetectable by CPL spectroscopy, we combined a luminescence spectrophotometer with an L/R-circular polarization filter (L/R-CPF) in the phosphorescence measurement mode to explore CPRTP behaviour.[65] In accordance with the definition of CPL, RTP dissymmetric factors (g_{RTP}) can be used to express the degree of CPRTP, which can be defined as

$$g_{RTP} = 2 \times (I_L - I_R)/(I_L + I_R)$$

where I_L and I_R are the intensities of RTP recorded under L-CPF and R-CPF, respectively. The RTP intensity of P-(R)-B-4-CzO recorded under the L-CPF filter was stronger than that recorded under the R-CPF (Fig. 7d), and the value of g_{RTP} could be calculated to be +0.054. This result agreed with the plus or minus of the g_{lum} value of the fluorescence CPL obtained from the JASCO CPL-200 spectrometer, which also proved the feasibility of this method. The results showed that the polymer network presented excellent CPRTP properties with a $|g_{RTP}| = 0.013 \sim 0.098$ for P-(R/S)-B-n-CzO (Fig. 7e and Fig. S6, ESI†). Meantime, the CPRTP chiral inversion has been observed similar to those in the fluorescence CPL behaviour, which also attributed to the presence of S-CPRTP in P-(R)-B-4-CzO and R-CPRTP in P-(S)-B-4-CzO. In order to verify the role of the crosslinked network structure in generating phosphorescent CPL, the CPL properties of commercial LC E7 doped with the compounds have been explored (Fig. S8–S11 and Table S1, ESI†). Since E7 was not a fluid without a crosslinking rigid network structure, the samples only exhibit fluorescence CPL but not phosphorescent CPL. Therefore, the cross-linked network structure played the key role in generating CPRTP.

Conclusions

In summary, a series of liquid crystalline polymer networks with CPRTP properties were successfully prepared through *in situ* cross-linking the mixture of a liquid crystalline monomer and a luminescent compound. The liquid crystalline monomer not only self-assembles into a long-range ordered structure to amplify the CPL signal, but also offers a preferred rigid environment to restrict molecular motion and reduce the non-radiative transition of the luminescent compound after polymerization, which resulted in promoting the generation of CPRTP with a maximum g_{RTP} value of +0.098. This work successfully provided a strategy for the preparation of excellent CPRTP materials with high g_{lum} values, which could extend their applications in optical material fields.

Author contributions

Ao Huang carried out the experiments of the synthesis and photophysical properties, and writing the manuscript; Jiang Huang performed the circularly polarized luminescence experiment; Hui-Ying Luo and Zhi-Wang Luo performed the analysis of the data; Pu Wang performed theoretical calculations; Ping Wang participated in the molecular design and revised the manuscript; Yan Guan performed the fluorescence quantum yields and lifetime decay curve experiment; He-Lou Xie designed the project and organized and revised the manuscript. All authors critically commented on the project.

Conflicts of interest

There are no conflicts to declare.

Acknowledgements

Notes and references

1 C. He, G. Yang, Y. Kuai, S. Shan, L. Yang, J. Hu, D. Zhang, Q. Zhang and G. Zou, *Nat. Commun.*, 2018, **9**, 5117.

2 H.-C. Ma, G.-J. Chen, F. Huang and Y.-B. Dong, *J. Am. Chem. Soc.*, 2020, **142**, 12574–12578.

3 Y. Ai, Y. Fei, Z. Shu, Y. Zhu, J. Liu and Y. Li, *Chem. Eng. J.*, 2022, **450**, 138390.

4 Y. Sang, J. Han, T. Zhao, P. Duan and M. Liu, *Adv. Mater.*, 2020, **32**, 1900110.

5 X. Zhan, F.-F. Xu, Z. Zhou, Y. Yan, J. Yao and Y. S. Zhao, *Adv. Mater.*, 2021, **33**, 2104418.

6 D. Zhao, H. He, X. Gu, L. Guo, K. S. Wong, J. W. Y. Lam and B. Z. Tang, *Adv. Opt. Mater.*, 2016, **4**, 534–539.

7 Y. Dong, H. Zhao, S. Wang, Q. Cheng, S. Liu and Y. Li, *ACS Appl. Mater. Interfaces*, 2022, **14**, 40313–40321.

8 S. Lin, S. Zeng, Z. Li, Q. Fan and J. Guo, *ACS Appl. Mater. Interfaces*, 2022, **14**, 30362–30370.

This journal is © The Royal Society of Chemistry 2023

J. Mater. Chem. C, 2023, **11**, 4104–4111 | **4109**

9 Q. Xia, W. Xie, T. He, H. Zhang, Z. Zhao, G. Huang, S. Li Bing and Z. Tang Ben, *CCS Chem.*, 2022, **0**, 1–11.

10 Y. Deng, M. Wang, Y. Zhuang, S. Liu, W. Huang and Q. Zhao, *Light: Sci. Appl.*, 2021, **10**, 76.

11 Z.-L. Gong, X. Zhu, Z. Zhou, S.-W. Zhang, D. Yang, B. Zhao, Y.-P. Zhang, J. Deng, Y. Cheng, Y.-X. Zheng, S.-Q. Zang, H. Kuang, P. Duan, M. Yuan, C.-F. Chen, Y. S. Zhao, Y.-W. Zhong, B. Z. Tang and M. Liu, *Sci. China: Chem.*, 2021, **64**, 2060–2104.

12 F. Song, Z. Zhao, Z. Liu, J. W. Y. Lam and B. Z. Tang, *J. Mater. Chem. C*, 2020, **8**, 3284–3301.

13 Y. Wu, C. Yan, X.-S. Li, L. H. You, Z.-Q. Yu, X. Wu, Z. Zheng, G. Liu, Z. Guo, H. Tian and W.-H. Zhu, *Angew. Chem., Int. Ed.*, 2021, **60**, 24549–24557.

14 J. Han, S. Guo, H. Lu, S. Liu, Q. Zhao and W. Huang, *Adv. Opt. Mater.*, 2018, **6**, 1800538.

15 E. M. Sánchez-Carnerero, A. R. Agarrabeitia, F. Moreno, B. L. Maroto, G. Muller, M. J. Ortiz and S. de la Moya, *Chem. – Eur. J.*, 2015, **21**, 13488–13500.

16 Y. He, S. Lin, J. Guo and Q. Li, *Aggregate*, 2021, **2**, e141.

17 X.-Y. Luo and M. Pan, *Coord. Chem. Rev.*, 2022, **468**, 214640.

18 D.-M. Lee, J.-W. Song, Y.-J. Lee, C.-J. Yu and J.-H. Kim, *Adv. Mater.*, 2017, **29**, 1700907.

19 J. L. Greenfield, J. Wade, J. R. Brandt, X. Shi, T. J. Penfold and M. J. Fuchter, *Chem. Sci.*, 2021, **12**, 8589–8602.

20 K. Zuo, H. Shi, X. Yan, J. Liu, Y.-J. Liu, D. Luo and Y. Shi, *J. Mater. Chem. C*, 2022, **10**, 14729–14736.

21 S. Mukherjee and P. Thilagar, *Chem. Commun.*, 2015, **51**, 10988–11003.

22 S. Xu, R. Chen, C. Zheng and W. Huang, *Adv. Mater.*, 2016, **28**, 9920–9940.

23 W. Zhao, Z. He and B. Z. Tang, *Nat. Rev. Mater.*, 2020, **5**, 869–885.

24 O. Bolton, K. Lee, H.-J. Kim, K. Y. Lin and J. Kim, *Nat. Chem.*, 2011, **3**, 205–210.

25 L. Gu, H. Shi, L. Bian, M. Gu, K. Ling, X. Wang, H. Ma, S. Cai, W. Ning, L. Fu, H. Wang, S. Wang, Y. Gao, W. Yao, F. Huo, Y. Tao, Z. An, X. Liu and W. Huang, *Nat. Photonics*, 2019, **13**, 406–411.

26 L. Gu, H. Shi, M. Gu, K. Ling, H. Ma, S. Cai, L. Song, C. Ma, H. Li, G. Xing, X. Hang, J. Li, Y. Gao, W. Yao, Z. Shuai, Z. An, X. Liu and W. Huang, *Angew. Chem., Int. Ed.*, 2018, **57**, 8425–8431.

27 Z. He, W. Zhao, J. W. Y. Lam, Q. Peng, H. Ma, G. Liang, Z. Shuai and B. Z. Tang, *Nat. Commun.*, 2017, **8**, 416.

28 K. Jiang, Y. Wang, C. Cai and H. Lin, *Adv. Mater.*, 2018, **30**, 1800783.

29 X. Kong, X. Wang, H. Cheng, Y. Zhao and W. Shi, *J. Mater. Chem. C*, 2019, **7**, 230–236.

30 Z. Yang, Z. Mao, X. Zhang, D. Ou, Y. Mu, Y. Zhang, C. Zhao, S. Liu, Z. Chi, J. Xu, Y.-C. Wu, P.-Y. Lu, A. Lien and M. R. Bryce, *Angew. Chem., Int. Ed.*, 2016, **55**, 2181–2185.

31 Z. Yang, C. Xu, W. Li, Z. Mao, X. Ge, Q. Huang, H. Deng, J. Zhao, F. L. Gu, Y. Zhang and Z. Chi, *Angew. Chem., Int. Ed.*, 2020, **59**, 17451–17455.

32 W. Z. Yuan, X. Y. Shen, H. Zhao, J. W. Y. Lam, L. Tang, P. Lu, C. Wang, Y. Liu, Z. Wang, Q. Zheng, J. Z. Sun, Y. Ma and B. Z. Tang, *J. Phys. Chem. C*, 2010, **114**, 6090–6099.

33 Y. Fan, M. Han, A. Huang, Q. Liao, J. Tu, X. Liu, B. Huang, Q. Li and Z. Li, *Mater. Horiz.*, 2022, **9**, 368–375.

34 N. Gan, H. Shi, Z. An and W. Huang, *Adv. Funct. Mater.*, 2018, **28**, 1802657.

35 S. Hirata, K. Totani, J. Zhang, T. Yamashita, H. Kaji, S. R. Marder, T. Watanabe and C. Adachi, *Adv. Funct. Mater.*, 2013, **23**, 3386–3397.

36 R. Kabe, N. Notsuka, K. Yoshida and C. Adachi, *Adv. Mater.*, 2016, **28**, 655–660.

37 T. Ogoshi, H. Tsuchida, T. Kakuta, T.-A. Yamagishi, A. Taema, T. Ono, M. Sugimoto and M. Mizuno, *Adv. Funct. Mater.*, 2018, **28**, 1707369.

38 Y. Su, S. Z. F. Phua, Y. Li, X. Zhou, D. Jana, G. Liu, W. Q. Lim, W. K. Ong, C. Yang and Y. Zhao, *Sci. Adv.*, 2018, **4**, eaas9732.

39 Z. An, C. Zheng, Y. Tao, R. Chen, H. Shi, T. Chen, Z. Wang, H. Li, R. Deng, X. Liu and W. Huang, *Nat. Mater.*, 2015, **14**, 685–690.

40 J. Wang, X. Gu, H. Ma, Q. Peng, X. Huang, X. Zheng, S. H. P. Sung, G. Shan, J. W. Y. Lam, Z. Shuai and B. Z. Tang, *Nat. Commun.*, 2018, **9**, 2963.

41 X. Zhang, L. Du, W. Zhao, Z. Zhao, Y. Xiong, X. He, P. F. Gao, P. Alam, C. Wang, Z. Li, J. Leng, J. Liu, C. Zhou, J. W. Y. Lam, D. L. Phillips, G. Zhang and B. Z. Tang, *Nat. Commun.*, 2019, **10**, 5161.

42 Y. Zhou, W. Qin, C. Du, H. Gao, F. Zhu and G. Liang, *Angew. Chem., Int. Ed.*, 2019, **58**, 12102–12106.

43 S. An, L. Gao, A. Hao and P. Xing, *ACS Nano*, 2021, **15**, 20192–20202.

44 W. Chen, Z. Tian, Y. Li, Y. Jiang, M. Liu and P. Duan, *Chem. – Eur. J.*, 2018, **24**, 17444–17448.

45 W. Hao, Y. Li and M. Liu, *Adv. Opt. Mater.*, 2021, **9**, 2100452.

46 H. Li, J. Gu, Z. Wang, J. Wang, F. He, P. Li, Y. Tao, H. Li, G. Xie, W. Huang, C. Zheng and R. Chen, *Nat. Commun.*, 2022, **13**, 429.

47 H. Li, H. Li, W. Wang, Y. Tao, S. Wang, Q. Yang, Y. Jiang, C. Zheng, W. Huang and R. Chen, *Angew. Chem., Int. Ed.*, 2020, **59**, 4756–4762.

48 R. Liu, B. Ding, D. Liu and X. Ma, *Chem. Eng. J.*, 2021, **421**, 129732.

49 D. Zhang, H. Zheng, X. Ma, L. Su, X. Gao, Z. Tang and Y. Xu, *Adv. Opt. Mater.*, 2022, **10**, 2102015.

50 Y. Jiang, W. Su, G. Li, Y. Fu, Z. Li, M. Qin and Z. Yuan, *Chem. Eng. J.*, 2022, **430**, 132780.

51 Z.-W. Luo, L. Tao, C.-L. Zhong, Z.-X. Li, K. Lan, Y. Feng, P. Wang and H.-L. Xie, *Macromolecules*, 2020, **53**, 9758–9768.

52 Y. Zhang, H. Li, Z. Geng, W.-H. Zheng, Y. Quan and Y. Cheng, *ACS Nano*, 2022, **16**, 3173–3181.

53 J. Park, T. Yu, T. Inagaki and K. Akagi, *Macromolecules*, 2015, **48**, 1930–1940.

54 X. Yang, X. Jin, T. Zhao and P. Duan, *Mater. Chem. Front.*, 2021, **5**, 4821–4832.

55 Y. Zhu, Y. Guan, Y. Niu, P. Wang, R. Chen, Y. Wang, P. Wang and H.-L. Xie, *Adv. Opt. Mater.*, 2021, **9**, 2100782.

56 Z. Geng, Y. Zhang, Y. Zhang, Y. Quan and Y. Cheng, *Angew. Chem., Int. Ed.*, 2022, **61**, e202202718.

57 G. Chen, W. Li, T. Zhou, Q. Peng, D. Zhai, H. Li, W. Z. Yuan, Y. Zhang and B. Z. Tang, *Adv. Mater.*, 2015, **27**, 4496–4501.

58 H. Wu, Z. Chen, W. Chi, A. K. Bindra, L. Gu, C. Qian, B. Wu, B. Yue, G. Liu, G. Yang, L. Zhu and Y. Zhao, *Angew. Chem., Int. Ed.*, 2019, **58**, 11419–11423.

59 L. Zou, S. Guo, H. Lv, F. Chen, L. Wei, Y. Gong, Y. Liu and C. Wei, *Dyes Pigm.*, 2022, **198**, 109958.

4110 | *J. Mater. Chem. C*, 2023, **11**, 4104–4111

This journal is © The Royal Society of Chemistry 2023

60 R. Chen, Y. Guan, H. Wang, Y. Zhu, X. Tan, P. Wang, X. Wang, X. Fan and H.-L. Xie, *ACS Appl. Mater. Interfaces*, 2021, **13**, 41131–41139.

61 G. Bergamini, A. Fermi, C. Botta, U. Giovanella, S. Di Motta, F. Negri, R. Peresutti, M. Gingras and P. Ceroni, *J. Mater. Chem. C*, 2013, **1**, 2717–2724.

62 L. Gu, W. Ye, X. Liang, A. Lv, H. Ma, M. Singh, W. Jia, Z. Shen, Y. Guo, Y. Gao, H. Chen, D. Wang, Y. Wu, J. Liu, H. Wang, Y.-X. Zheng, Z. An, W. Huang and Y. Zhao, *J. Am. Chem. Soc.*, 2021, **143**, 18527–18535.

63 Z.-A. Yan, X. Lin, S. Sun, X. Ma and H. Tian, *Angew. Chem., Int. Ed.*, 2021, **60**, 19735–19739.

64 X. Gao, X. Qin, X. Yang, Y. Li and P. Duan, *Chem. Commun.*, 2019, **55**, 5914–5917.

65 M. Xu, X. Wu, Y. Yang, C. Ma, W. Li, H. Yu, Z. Chen, J. Li, K. Zhang and S. Liu, *ACS Nano*, 2020, **14**, 11130–11139.

This journal is © The Royal Society of Chemistry 2023

J. Mater. Chem. C, 2023, **11**, 4104–4111 | **4111**